

# OPTIMIZATION OF THE LUCY INTERPLANETARY TRAJECTORY VIA TWO-POINT DIRECT SHOOTING

Jacob A. Englander\*  
Donald H. Ellison†  
Ken Williams‡  
James McAdams§  
Jeremy M. Knittel¶  
Brian Sutter||  
Chelsea Welch\*\*  
Dale Stanbridge††  
Kevin Berry‡‡

Lucy is NASA’s next Discovery-class mission and will explore the Trojan asteroids in the Sun-Jupiter L4 and L5 regions. This paper details the design of Lucy’s interplanetary trajectory using a two-point direct shooting transcription, nonlinear programming, and monotonic basin hopping. These techniques are implemented in the Evolutionary Mission Trajectory Generator (EMTG), a trajectory optimization tool developed at NASA Goddard Space Flight Center. We present applications to the baseline trajectory design, Monte Carlo analysis, and operations.

## INTRODUCTION

Lucy is NASA’s next Discovery-class planetary science mission. Lucy will launch in 2021 and will explore the bodies known as “Trojans” that orbit the Sun at the stable L4 and L5 points ahead and behind Jupiter. According to the Nice model of solar system formation, the Trojans may be remnants of the early solar system that were transported inward as the gas giants migrated outward [1]. When observed by telescope, the Trojans spectrally resemble Kuiper Belt object (KBO)s. Unlike KBOs, the Trojans are readily accessible and are therefore our best window back in time to see what the solar system originally looked like. Lucy will visit five of these objects: four at L4 and one, the binary pair Patroclus-Menoetius, at L5.

This paper describes the optimization of the Lucy trajectory using a two-point direct shooting method in the Evolutionary Mission Trajectory Generator (EMTG) version 9, a modular, scalable-fidelity trajectory optimization tool. EMTG can perform global search and trade studies in low fidelity and also optimize point solutions in sufficiently high fidelity that the EMTG solutions may

\*Aerospace Engineer, Navigation and Mission Design Branch, NASA Goddard Space Flight Center

†Aerospace Engineer, Navigation and Mission Design Branch, NASA Goddard Space Flight Center

‡Flight Director, Space Navigation and Flight Dynamics Practice, KinetX Aerospace, Simi Valley, California

§Aerospace Engineer, Space Navigation and Flight Dynamics Practice, KinetX Aerospace, Simi Valley, California

¶Aerospace Engineer, Space Navigation and Flight Dynamics Practice, KinetX Aerospace, Simi Valley, California

||Totally Awesome Trajectory Genius, Lockheed Martin Space Systems, Littleton, CO

\*\*Fantastically Awesome Deputy Trajectory Genius, Lockheed Martin Space Systems, Littleton, CO

††Lucy Navigation Team Chief, KinetX Aerospace, Simi Valley, CA

‡‡Lucy Flight Dynamics Lead, Navigation and Mission Design Branch, NASA Goddard Space Flight Center

be re-targeted in an operational navigation tool such as Multiple Interferometric Ranging Analysis using GPS Ensemble (MIRAGE). In its lowest-fidelity mode, EMTG is used to design Lucy with two-body dynamics, a two-point direct shooting transcription, and a patched-conic flyby transcription [2]. This type of analysis can be done very quickly and across a broad search space.

Once a set of low-fidelity solutions is generated, the trajectory is then re-optimized using the same two-point direct shooting for the interplanetary trajectory phases,  $n$ -body gravity, solar radiation pressure (SRP), and a high-fidelity model of the Earth gravity assist maneuvers [3]. Additional constraints are added to prevent the spacecraft from passing too close to the Sun during interplanetary phases and the Moon while inside the Earth’s sphere of influence. EMTG provides analytical partial derivatives for all of the problem constraints [4], enabling rapid and robust convergence.

The optimization techniques described in this work are applied to Lucy in several different ways. First, the baseline trajectory is periodically redesigned to take into account changes in the spacecraft design or new constraints. This redesign is done by first optimizing the trajectory in low and then high fidelity in EMTG, and then using the high-fidelity solution as an initial guess for re-optimization in Systems Tool Kit (STK) [5]. Second, EMTG’s high-fidelity mode is used to successively re-optimize the mission-to-go after each major maneuver in a Monte Carlo analysis. The EMTG results are then re-targeted in MIRAGE. The motivation for and results of this process are described in detail by McAdams et al. [6]. Third, EMTG is used to optimize the trajectory for each day in the primary launch period. These trajectories are then verified in General Mission Analysis Toolkit (GMAT) [7] using an automated process developed by the authors. Finally, we plan to use EMTG to generate initial guesses for each maneuver during operations. Just as in the Monte Carlo analysis, all EMTG solutions will be re-targeted in MIRAGE before any commands are sent to the spacecraft.

## PHYSICS MODEL

### Multiple Gravity Assist with $n$ Deep-Space Maneuvers

The trajectory transcription used in this work is EMTG’s Multiple Gravity Assist with  $n$  Deep-Space Maneuvers using Shooting (MGAnDSMs) [2, 8]. This transcription can model a trajectory with any number of impulsive maneuvers. MGAnDSMs models the trajectory between two boundary points as a two-point shooting phase. The trajectory is propagated forward in time from the left-hand boundary condition and backward in time from the right-hand boundary condition. The optimizer chooses the time of flight ( $TOF$ ) for the phase, along with necessary parameters to define the magnitude and direction of any impulsive deep-space maneuver (DSM)s. The  $TOF$  from the left-hand boundary to the first DSM, as well as from each DSM to the next DSM or to the right-hand boundary where appropriate, is expressed as the product of a “burn index”  $\eta_i$  with the phase  $TOF$ . The sum of the  $\eta_i$  must equal 1.0, guaranteeing that the propagation arcs fit within the phase  $TOF$ . Therefore, if a phase has only one impulse, then the time from the left boundary to the DSM,  $\Delta t_1$ , and the time from the DSM to the right boundary,  $\Delta t_2$  will be:

$$\Delta t_1 = \eta_1 TOF \tag{1}$$

$$\Delta t_2 = \eta_2 TOF \tag{2}$$

Mass is propagated across each impulse by means of the exponential form of the rocket equation as shown in Equation 3.

$$m_i^+ = m_i^- \exp\left(\frac{-\Delta v}{I_{sp} g_0}\right) \tag{3}$$

where  $m_i^-$  is the mass of the spacecraft before the maneuver,  $m_i^+$  is the mass of the spacecraft after

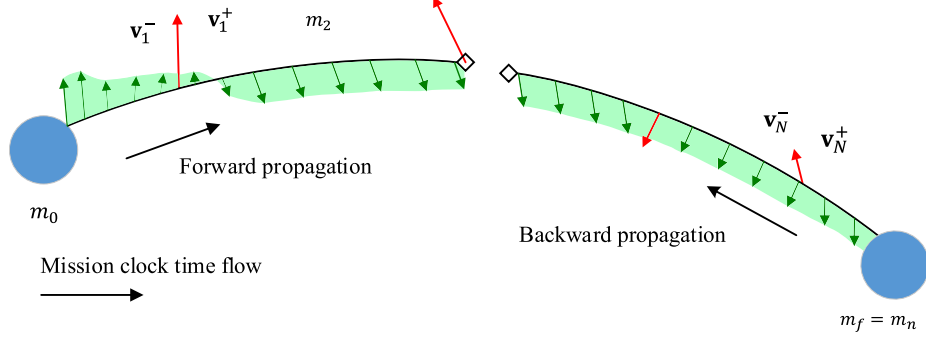


Figure 1: Diagram of the MGAnDSMs transcription. The red arrows represent impulsive DSMs, and the green-highlighted black arrows represent natural perturbations.

Table 1: Decision variables that define an MGAnDSMs phase

Variable	Description
$TOF$	time-of-flight of the phase
$\eta_i$	Fractions of the phase $TOF$ that define the time between DSMs and the boundaries, as well as between DSMs and other DSMs. One per DSM plus one for the right-hand boundary.
$\Delta v_{i,x}$	$x$ component of DSM $i$ . One per DSM
$\Delta v_{i,y}$	$y$ component of DSM $i$ . One per DSM
$\Delta v_{i,z}$	$z$ component of DSM $i$ . One per DSM

the maneuver,  $\Delta v$  is the magnitude of the impulsive DSM,  $g_0$  is the acceleration due to gravity at sea level on Earth, and  $I_{sp}$  is the specific impulse of the spacecraft's thruster.

The decision variables and constraints necessary to define an MGAnDSMs phase are listed in Tables 1 and 2, respectively. A diagram of the MGAnDSMs phase architecture is shown in Figure 1. The subscript  $m_p$  denotes that a given constraint is expressed at the match point.

### Dynamics and Propagation

The low-fidelity trajectories in this work are modeled using two-body dynamics and propagated by solving Kepler's problem. EMTG uses a universal-variable formulation, combined with a variable-order Laguerre root finder [9, 10].

The high-fidelity trajectories in this work are modeled using an  $n$ -body point mass gravity model,

Table 2: Constraints that define an MGAnDSMs phase.

Constraint	Depends on
$x_{mp}^+ = x_{mp}^-$	$TOF$ , all $\eta_i$ , all $\Delta v_{i,x}$ , all $\Delta v_{i,y}$ , all $\Delta v_{i,z}$ , boundary variables
$y_{mp}^+ = y_{mp}^-$	$TOF$ , all $\eta_i$ , all $\Delta v_{i,x}$ , all $\Delta v_{i,y}$ , all $\Delta v_{i,z}$ , boundary variables
$z_{mp}^+ = z_{mp}^-$	$TOF$ , all $\eta_i$ , all $\Delta v_{i,x}$ , all $\Delta v_{i,y}$ , all $\Delta v_{i,z}$ , boundary variables
$\dot{x}_{mp}^+ = \dot{x}_{mp}^-$	$TOF$ , all $\eta_i$ , all $\Delta v_{i,x}$ , all $\Delta v_{i,y}$ , all $\Delta v_{i,z}$ , boundary variables
$\dot{y}_{mp}^+ = \dot{y}_{mp}^-$	$TOF$ , all $\eta_i$ , all $\Delta v_{i,x}$ , all $\Delta v_{i,y}$ , all $\Delta v_{i,z}$ , boundary variables
$\dot{z}_{mp}^+ = \dot{z}_{mp}^-$	$TOF$ , all $\eta_i$ , all $\Delta v_{i,x}$ , all $\Delta v_{i,y}$ , all $\Delta v_{i,z}$ , boundary variables
$m_{mp}^+ = m_{mp}^-$	$TOF$ , all $\eta_i$ , all $\Delta v_{i,x}$ , all $\Delta v_{i,y}$ , all $\Delta v_{i,z}$ , boundary variables
$\sum_{i=1}^{n+1} \eta_i = 1.0$	all $\eta_i$

Table 3: Decision variables that define a patched-conic launch

Variable	Description
$t_{launch}$	epoch of launch
$v_{\infty}$	magnitude of the outgoing velocity asymptote
$RLA$	right ascension of the outgoing velocity asymptote in ICRF
$DLA$	declination of the outgoing velocity asymptote in ICRF

the  $J_2$  term of the central body (e.g. the Sun or the Earth), and solar radiation pressure. The model used for this work includes all eight planets, Pluto, and Earth’s moon as drawn from the DE430 ephemeris [11]. EMTG propagates these trajectories with an 8th-order fixed-step Runge-Kutta explicit integrator [?]. Using a fixed-step integrator ensures that the analytical partial derivatives of the final state with respect to the initial state and the time of integration are exact [?].

### Launch

In low fidelity, EMTG uses a patched-conic, zero-sphere of influence (SOI) approximation of launch. The optimizer chooses the launch epoch and the outgoing  $v_{\infty}$ , Right Ascension of Launch Asymptote (RLA), and Declination of Launch Asymptote (DLA) as shown in Table 3. The patched-conic launch model does not add any constraints to the problem. The initial state of the spacecraft in the heliocentric reference frame is then computed at the center of the launch body as per Equations 4-11. The coefficients in Equation 11 are a polynomial fit to the performance of the actual launch vehicle, which in the case of Lucy is an Atlas V 401.

$$C_3 = v_{\infty}^2 \tag{4}$$

$$x_0 = x_{body}(t_{launch}) \tag{5}$$

$$y_0 = y_{body}(t_{launch}) \tag{6}$$

$$z_0 = z_{body}(t_{launch}) \tag{7}$$

$$\dot{x}_0 = \dot{x}_{body}(t_{launch}) + C_3 \cos RLA \cos DLA \tag{8}$$

$$\dot{y}_0 = \dot{y}_{body}(t_{launch}) + C_3 \sin RLA \cos DLA \tag{9}$$

$$\dot{z}_0 = \dot{z}_{body}(t_{launch}) + C_3 \sin DLA \tag{10}$$

$$m_0 = a_{LV} + b_{LV}C_3 + c_{LV}C_3^2 + d_{LV}C_3^3 + e_{LV}C_3^4 + f_{LV}C_3^5 \tag{11}$$

When EMTG is used to optimize Lucy in high fidelity, the launch is modeled by an impulsive departure from a circular parking orbit at 185 km altitude. EMTG then propagates from the departure maneuver to the point at which Lucy exits the SOI of the Earth. This process introduces additional decision variables and constraints, but a complete discussion is out of scope for this paper. A full description may be found in the companion paper by Ellison et al. [3].

### Gravity Assist Model

EMTG uses two different models for Lucy’s Earth gravity assists, depending on the fidelity of the simulation. In low fidelity, EMTG uses a patched-conic, zero-SOI approximation that is common to many preliminary design tools. This is done by adding six new decision variables, defining the incoming and outgoing  $v_{\infty}$ , and two new constraints: one to require that the magnitude of  $v_{\infty,out}$  matches the magnitude of  $v_{\infty,in}$ , and one to ensure that the bend angle does not require the spacecraft to fly below a user-defined safe distance  $h_{safe}$  from the body, as described in Equations 12-14, where  $F$  is the constraint posed to the optimizer. The decision variables are listed in Table 4, and the constraints are listed in Table 5. In the context of Lucy,  $h_{safe}$  is 300 km. The flyby is un-powered, i.e., no maneuver occurs at periapse.

Table 4: Decision variables that define a patched-conic flyby

Variable	Description
$v_{\infty,in,x}$	$x$ component of incoming velocity vector
$v_{\infty,in,y}$	$y$ component of incoming velocity vector
$v_{\infty,in,z}$	$z$ component of incoming velocity vector
$v_{\infty,out,x}$	$x$ component of outgoing velocity vector
$v_{\infty,out,y}$	$y$ component of outgoing velocity vector
$v_{\infty,out,z}$	$z$ component of outgoing velocity vector

Table 5: Constraints that define a patched-conic flyby

Constraint	Depends on
$\ \mathbf{v}_{\infty-in}\  = \ \mathbf{v}_{\infty-out}\ $	$v_{\infty-in-x}, v_{\infty-in-y}, v_{\infty-in-z}, v_{\infty-out-x}, v_{\infty-out-y}, v_{\infty-out-z}$
$h \geq h_{safe}$	$v_{\infty-in-x}, v_{\infty-in-y}, v_{\infty-in-z}, v_{\infty-out-x}, v_{\infty-out-y}, v_{\infty-out-z}$

$$F = h_{FB} - h_{safe} \quad (12)$$

$$h_{FB} = \frac{\mu}{v_{\infty,out}^2} \left( \frac{1}{\sin \frac{\delta_{FB}}{2}} - 1 \right) - r_{body} \quad (13)$$

$$\delta_{FB} = \arccos \left( \frac{\mathbf{v}_{\infty,out} \bullet \mathbf{v}_{\infty,in}}{v_{\infty,out} v_{\infty,in}} \right) \quad (14)$$

When EMTG is used to optimize Lucy in high fidelity, the gravity assist maneuvers are modeled by propagating through the finite SOI of the Earth, with the Earth as the central body. This process introduces additional decision variables and constraints, but a complete discussion is out of scope for this paper. A full description may be found in the companion paper by Ellison et al. [3].

#### Encounter Model

EMTG models the Trojan and Donaldjohanson encounters as an intercept, i.e, a match of the precise position of the body but with a non-zero  $\mathbf{v}_{\infty}$  vector. Since the Trojans and Donaldjohanson are very small, EMTG does not model a bend angle. EMTG encodes six decision variables describing the incoming and outgoing velocity vectors, as described in Table 6, and three constraints to ensure that the incoming and outgoing velocity vectors are identical, as described in Table 7. This model is used in both the low- and high-fidelity Lucy results in this work, and yields a trajectory accurate enough to be re-targeted in MIRAGE with more precise encounter modeling.

Table 6: Decision variables that define a small-body flyby

Variable	Description
$v_{\infty,in,x}$	$x$ component of incoming velocity vector
$v_{\infty,in,y}$	$y$ component of incoming velocity vector
$v_{\infty,in,z}$	$z$ component of incoming velocity vector
$v_{\infty,out,x}$	$x$ component of outgoing velocity vector
$v_{\infty,out,y}$	$y$ component of outgoing velocity vector
$v_{\infty,out,z}$	$z$ component of outgoing velocity vector

Table 7: Constraints that define a small-body flyby

Constraint	Depends on
$v_{\infty,in,x} = v_{\infty,out,x}$	$v_{\infty,in,x}, v_{\infty,out,x}$
$v_{\infty,in,z} = v_{\infty,out,y}$	$v_{\infty,in,y}, v_{\infty,out,y}$
$v_{\infty,in,z} = v_{\infty,out,z}$	$v_{\infty,in,z}, v_{\infty,out,z}$

## SOLVER

### Nonlinear Programming

The optimization of the MGA<sub>n</sub>DSMs problems in this work may be formulated as nonlinear program (NLP) problems. The optimizer solves a problem of the form:

$$\begin{aligned}
 & \text{Minimize } f(\mathbf{x}) \\
 & \text{Subject to:} \\
 & \mathbf{x}_{lb} \leq \mathbf{x} \leq \mathbf{x}_{ub} \\
 & \mathbf{c}(\mathbf{x}) \leq \mathbf{0} \\
 & A\mathbf{x} \leq \mathbf{0}
 \end{aligned} \tag{15}$$

where  $\mathbf{x}_{lb}$  and  $\mathbf{x}_{ub}$  are the lower and upper bounds on the decision vector,  $\mathbf{c}(\mathbf{x})$  is a vector of nonlinear constraint functions, and  $A$  is a matrix describing any linear constraints (e.g. time constraints).

The problems in this work, like most other interplanetary trajectory optimization problems, consist of hundreds of variables and tens to hundreds of constraints. Such problems are best solved with a sparse NLP solver such as Sparse Nonlinear OPTimizer (SNOPT) [12]. SNOPT uses a sparse sequential quadratic programming (SQP) method and benefits greatly from precise knowledge of the problem Jacobian, i.e., the matrix of partial derivatives of the objective function and constraints with respect to the decision variables. EMTG provides analytical expressions for all of the necessary partial derivatives, leading to improved convergence vs. using numerically approximated derivatives [4, 8, 13]. SNOPT, like all NLP solvers, requires an initial guess of the solution and tends to converge to a solution in the neighborhood of that initial guess. The next section discusses EMTG’s fully automated method for generating initial guesses.

### Monotonic Basin Hopping

In the past two decades, researchers have explored stochastic search methods that do not require an initial guess. Stochastic search techniques allow an automated system to efficiently design a complex trajectory without human input [2, 14–24]. EMTG is designed to operate without user oversight, and so relies heavily upon stochastic search. The particular stochastic search method used in this work is monotonic basin hopping (MBH).

MBH [25] is an algorithm for searching for the best solutions to problems with many local optima. Many problems, including those described in this work, are structured such that individual locally optimal “basins” cluster together, where the distance in the decision space from one local optima to the next in a given cluster may be traversed in a short “hop.” A problem may have several such clusters. MBH was originally developed to solve molecular conformation problems in computational chemistry, but has been demonstrated to be effective on various types of interplanetary trajectory problems [14, 20–22, 26, 27]. Pseudocode for MBH is given in Algorithm 1.

Special attention is given to decision variables that define the time-of-flight between two boundary points, e.g. Earth or Trojan flybys in Lucy. These are the most significant variables that define a trajectory and therefore it is sometimes necessary to drastically perturb them in order to “hop” to a new cluster of solutions. With some (low) uniform-random probability  $\rho$ , each time-of-flight variables is shifted by  $\pm 1$  synodic period of the two boundary points defining that trajectory phase.

In preliminary design for Lucy,  $\rho$  was set to 0.05. In high fidelity re-optimization,  $\rho$  is set to 0.0, because we do not expect significant changes to the trajectory.

---

Algorithm 1 Monotonic Basin Hopping (MBH)

---

```

generate random point  $\mathbf{x}$ 
run NLP solver to find point  $\mathbf{x}^*$  using initial guess  $\mathbf{x}$ 
 $\mathbf{x}_{current} = \mathbf{x}^*$ 
if  $\mathbf{x}^*$  is a feasible point then
    save  $\mathbf{x}^*$  to archive
end if
while not hit stop criterion do
    generate  $\mathbf{x}'$  by randomly perturbing  $\mathbf{x}_{current}$ 
    for each time-of-flight variable  $t_i$  in  $\mathbf{x}'$  do
        if  $rand(0, 1) < \rho_{time-hop}$  then
            shift  $t_i$  forward or backward one synodic period
        end if
    end for
    run NLP solver to find locally optimal point  $\mathbf{x}^*$  using in initial guess  $\mathbf{x}'$ 
    if  $\mathbf{x}^*$  is feasible and  $f(\mathbf{x}^*) < f(\mathbf{x}_{current})$  then
         $\mathbf{x}_{current} = \mathbf{x}^*$ 
        save  $\mathbf{x}^*$  to archive
    else if  $\mathbf{x}^*$  is infeasible and  $\|c(\mathbf{x}^*)\| < \|c(\mathbf{x}_{current})\|$  then
         $\mathbf{x}_{current} = \mathbf{x}^*$ 
    end if
end while
return best  $\mathbf{x}^*$  in archive

```

---

MBH is run until either a specified number of iterations (trial points attempted) or a maximum CPU time is reached, at which point the best solution stored in the archive is returned. The version of MBH used in EMTG has two parameters: the stopping criterion and the type of random step used to generate the perturbed decision vector  $\mathbf{x}'$ . In this work, the random step is drawn from a bi-directional Pareto distribution with the Pareto parameter,  $\alpha$ , set to 1.4. The bi-directional Pareto distribution usually generates small steps that allow MBH to exploit the local cluster around the current best solution. However, some of the steps generated by the bi-directional Pareto distribution are much larger, in some cases spanning the entire decision space. These larger steps allow MBH to explore the full decision space. This approach has been shown to be robust on complex interplanetary trajectory design problems [24].

MBH may be started either from a uniform-randomly chosen point in the decision space or from an initial guess derived from a previous problem. As long as the two problems are sufficiently similar, the latter approach is more efficient than starting from randomness. This property is exploited in the following section.

#### Python EMTG Automated Trade Study Application (PEATSA)

EMTG is most often run in a large-scale search mode, in which there are tens-to-thousands of individual cases that must be optimized. One example, as described later in this work, is the case of mapping a launch period to generate an optimal solution at one-day, or finer, intervals. Another example is the case of re-optimizing the mission-to-go for thousands of Monte Carlo samples. While it is possible to perform an independent global search on each problem posed to EMTG using NLP and MBH as described above, it is greatly advantageous to exploit similarities between the cases and share information between EMTG runs.

In this work, we use EMTG in tandem with the Python EMTG Automated Trade Study Ap-

plication (PEATSA) wrapper script developed by Knittel et al. [28]. The user selects one or more variables by which solutions may be compared to each other, and the difference between the value(s) of these variable(s) define a “seed distance.” PEATSA harvests the results from a set of EMTG runs, and determines based on seed distance which EMTG solutions should be used to seed their neighbors. The EMTG cases are then re-run with each MBH process with the initial guesses locations chosen by PEATSA. After a short period of time (minutes), the EMTG runs are terminated and the seed-sharing process is repeated. This continues until either solutions to the population of cases cease to improve, the solutions all meet some user-defined threshold, or the analyst chooses to end the study.

## RESULTS

### Nominal Trajectory

The computational process described in the previous section is successfully applied to the Lucy mission. Lucy includes a launch, three Earth gravity assists, six small-body encounters, and nine MGA<sub>n</sub>DSMs phases. Figure 2 shows the problem structure as defined in EMTG.

The Lucy trajectory presented here, as developed for critical design review (CDR), was optimized first in EMTG’s low-fidelity mode, then in EMTG’s high-fidelity mode. The low-fidelity solution was used as a starting point for the high-fidelity optimization. The resulting high-fidelity EMTG trajectory was then re-targeted in MIRAGE. Table 8 shows how the solution for the open of the 21-day launch period differs between the tools. Note that the low-fidelity, patched conic EMTG run yields a lower  $\Delta v$  than the high-fidelity EMTG and MIRAGE runs because the low-fidelity run does not account for SRP or  $n$ -body perturbations.

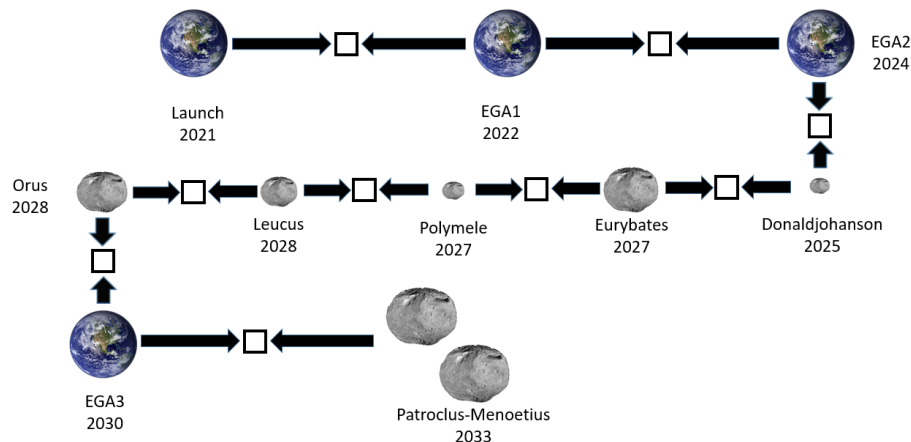


Figure 2: Structure of the Lucy mission

Figures 3 and 4 show the trajectory in an ecliptic plane projection and in a side view, respectively. From Figure 4, it is clear that Lucy’s Trojan asteroid targets lie in significantly different orbital planes. The Lucy mission is only possible because each of these targets cross the ecliptic plane in approximately the same place.

### Launch Period Optimization

Another application for the process described in this work is the optimization of a high-fidelity “launch vehicle target specification,” i.e., a table of  $C_3$ , RLA, and DLA targets across a 21-day launch period. This information is then provided to the launch vehicle flight dynamics team, who use the targets as terminal constraints for their optimization of the launch vehicle’s trajectory.

Table 8: Comparison of the low- and high-fidelity EMTG Lucy trajectories with the MIRAGE baseline, for the October 16th, 2021 launch opportunity.

Parameter	EMTG (low-fidelity)	EMTG (high-fidelity)	MIRAGE
Launch	10/16/2021	10/16/2021	10/16/2021
DSM1 epoch	4/23/2022	11/15/2021	11/15/2021
DSM1 (m/s)	2.1	3.8	3.5
EGA1 epoch	10/17/2022	10/16/2022	10/16/2022
EGA1 altitude (km)	300	300	283
DSM2 epoch	2/1/2024	2/7/2024	2/6/2024
DSM2 (m/s)	889.6	910.9	909.6
EGA2 epoch	12/13/2024	12/13/2024	12/13/2024
EGA2 altitude (km)	341	334	350
Donaldjohanson epoch	4/20/2025	4/20/2025	4/20/2025
DSM3 epoch	4/13/2027	4/7/2027	4/7/2027
DSM3 magnitude (m/s)	308.6	312.9	310.6
Eurybates epoch	8/12/2027	8/12/2027	8/12/2027
Polymele epoch	9/15/2027	9/15/2027	9/15/2027
DSM4 epoch	9/29/2027	9/29/2027	9/29/2027
DSM4 magnitude (m/s)	114.7	115.9	117.4
Leucus epoch	4/18/2028	4/18/2028	4/18/2028
DSM5 epoch	7/22/2028	7/23/2028	7/23/2028
DSM5 magnitude (m/s)	349.7	350.8	349.6
Orus epoch	11/11/2028	11/11/2028	11/11/2028
EGA3 epoch	12/27/2030	12/27/2030	12/27/2030
EGA3 altitude (km)	654	611	637
Patroclus epoch	3/3/2033	3/3/2033	3/3/2033
Total mission $\Delta v$ (m/s)	1664.7	1693.5	1696.8

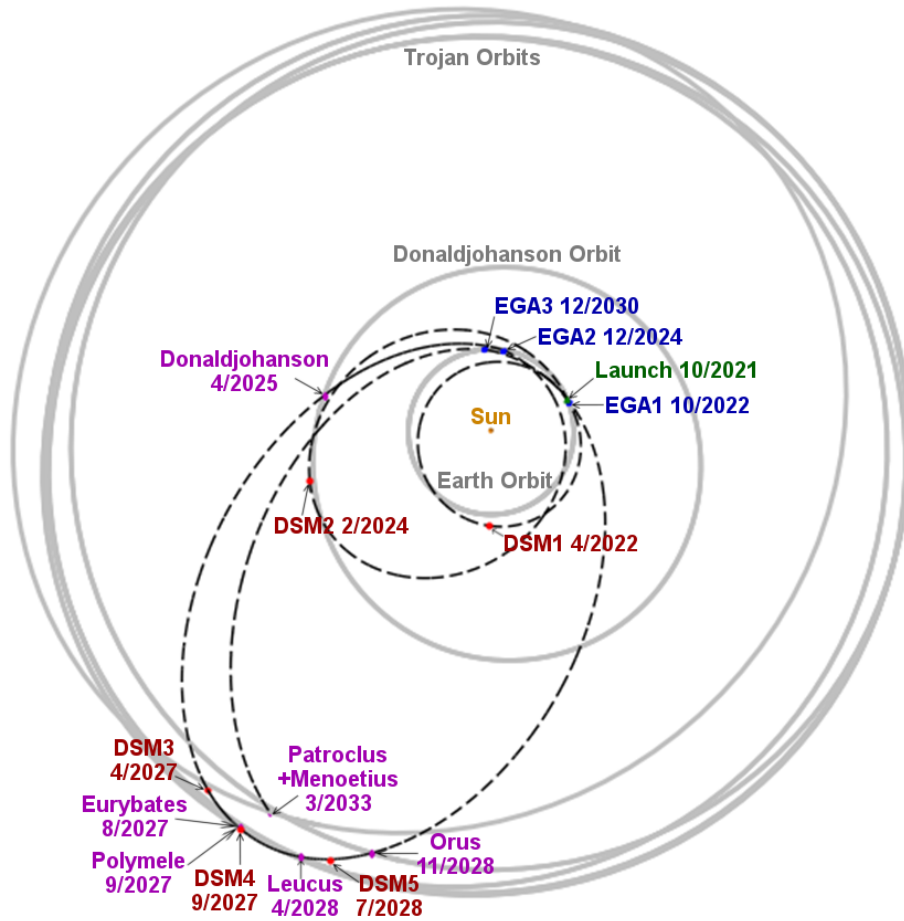


Figure 3: Ecliptic-plane projection of the Lucy baseline trajectory

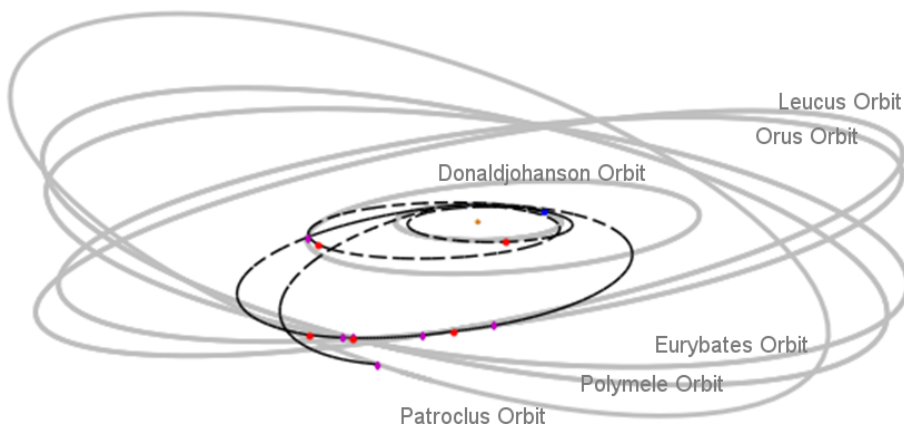


Figure 4: Side view of the Lucy baseline trajectory

The Lucy launch period optimization was performed using EMTG in its highest-fidelity mode, as described earlier in this work. Additional constraints were applied to the launch portion of the mission. First, it was necessary to prevent Lucy from passing too close to the Moon. Since the Moon’s orbit about the Earth is approximately circular and the launch hyperbola will cross the Moon’s orbital distance only once, it is sufficient to impose a constraint that “when the spacecraft reaches 384,000 km from the center of the Earth, it must also be at least 50,000 km from the Moon.” This was accomplished by breaking the portion of the trajectory from launch to Earth SOI exit into two phases: one before crossing the moon’s orbit, and one after. The boundary point between the phases is then constrained to be at exactly 384,000 km from the Earth and greater than or equal to 50,000 km from the Moon.

Second, the outbound hyperbola must be physically reachable by the launch vehicle. While the launch provider’s analysis is much more sophisticated and less constrained than the analysis here, it is sufficient for this work to impose a constraint that the spacecraft/launcher stack begins in a circular parking orbit that crosses the latitude and longitude of the launch site, Cape Canaveral Air Force Station (CCAFS) at an altitude of 185 km, and that the time between launch and hyperbolic injection be greater than the time that it takes the launch vehicle to reach that parking orbit. The first step is to constrain the initial orbit to an inclination of  $28.5^\circ$ , guaranteeing that the spacecraft passes over CCAFS. Next, we constrain the latitude and longitude of the injection maneuver such that it occurs approximately over the Indian Ocean –  $180^\circ$  of true anomaly after launch; enough time for the launch vehicle to ascend from the surface of the Earth to the parking orbit.

High-fidelity trajectories were optimized in EMTG for each day in the period from 10/16/2021 to 11/5/2021, subject to the constraints described above. These optimizations were carried out using the PEATSA process described in this work, and required no initial guess. Each trajectory was then re-targeted in the GMAT [7], using the EMTG trajectory as an initial guess. The GMAT solutions did not modify the launch asymptote, but rather re-targeted only the spacecraft’s maneuvers. The GMAT rendering is higher fidelity in the sense that EMTG models only the  $J_2$  term of the Earth’s non-spherical gravity and approximates all maneuvers as impulses, whereas GMAT models a  $50 \times 50$  Earth gravity field and finite burns. The results of this analysis, including the GMAT verification step, are shown in Table 9.

In general, the difference between the EMTG and GMAT solutions was very small, less than  $5 \text{ m/s}$  or 0.3% of the total mission  $\Delta v$ . There are several explanations for these differences. First, EMTG and GMAT use different force models, as previously described. Second, the two tools use different integrators - a fixed-step 8th-order Runge-Kutta for EMTG and an adaptive-step Runge-Kutta with 8th-order propagation and 9th-order error control for GMAT. Third, since we only forward target position coordinates in GMAT from the EMTG initial guess, resulting in 11 individual calls to GMAT’s differential corrector, differences between the two trajectories build up from one maneuver/target to the next. The latter is likely the biggest cause of the differences between the two tools. Fortunately, this would not be an issue in operations because we would re-optimize the mission-to-go after each maneuver is executed. Regardless, the GMAT step is a valuable verification that the launch asymptote coordinates are accurate and suitable for use in interfacing with the launch vehicle flight dynamics team.

## CONCLUSION

The two-point direct shooting transcription described in this work, when combined with either low- or high-fidelity physics models as appropriate for a given analysis, is a powerful tool for optimizing interplanetary cruise trajectories. The results presented here show the effectiveness of EMTG and PEATSA as part of the Lucy design process. As shown in this work, this technique is invaluable in performing early-stage design and in developing a set of target coordinates for the launch vehicle.

Table 9: Launch vehicle target specification and mission  $\Delta v$  across the primary launch period.

Date	$C_3$ [ $km^2/s^2$ ]	RLA [ $^\circ$ ]	DLA [ $^\circ$ ]	EMTG $\Delta v$ [ $m/s$ ]	GMAT $\Delta v$ [ $m/s$ ]	difference [ $m/s$ ]	difference [%]
10/16/2021	28.62876135	16.8	8.6	1690.5	1691.8	1.3	0.1%
10/17/2021	28.67983783	17.9	8.6	1667.3	1668.8	1.5	0.1%
10/18/2021	28.72026844	19.0	9.1	1645.3	1646.1	0.9	0.1%
10/19/2021	28.68516925	18.2	12.6	1625.7	1626.8	1.1	0.1%
10/20/2021	28.69115134	20.9	8.6	1608.4	1609.5	1.1	0.1%
10/21/2021	28.7420877	22.0	8.6	1594.8	1595.8	1.1	0.1%
10/22/2021	28.80194404	23.1	8.6	1584.6	1585.5	0.9	0.1%
10/23/2021	28.8817291	24.2	8.7	1578.2	1579.1	0.9	0.1%
10/24/2021	29.04366881	25.3	8.5	1575.2	1576.2	1.0	0.1%
10/25/2021	29.18388615	22.8	17.1	1574.1	1575.3	1.1	0.1%
10/26/2021	29.18363233	24.2	16.6	1580.6	1584.0	3.4	0.2%
10/27/2021	29.17938111	27.5	11.0	1586.1	1586.8	0.6	0.0%
10/28/2021	29.17996957	28.3	11.5	1595.9	1600.7	4.8	0.3%
10/29/2021	29.18033459	29.2	11.9	1606.0	1606.9	1.0	0.1%
10/30/2021	29.18064859	30.1	12.2	1616.7	1619.1	2.4	0.1%
10/31/2021	29.18101012	31.0	12.5	1628.2	1630.5	2.3	0.1%
11/1/2021	29.18132028	32.0	12.9	1640.4	1643.4	3.0	0.2%
11/2/2021	29.18160595	32.9	13.2	1653.2	1654.7	1.6	0.1%
11/3/2021	29.18186002	33.8	13.5	1666.5	1670.5	4.0	0.2%
11/4/2021	29.18209995	34.8	13.8	1680.3	1684.4	4.0	0.2%
11/5/2021	29.18231928	35.7	14.2	1694.6	1697.5	2.9	0.2%

## ACKNOWLEDGMENTS

The authors would like to acknowledge the Lucy project and the NASA Discovery program for funding this work. Jacob Englander and Donald Ellison would also like to acknowledge Professor Bruce Conway at the University of Illinois for overseeing the academic research that eventually evolved into the techniques and tool described in this work. We additionally acknowledge Matthew Vavrina for designing and building the initial version of the trajectory transcription that is used here.

## REFERENCES

- [1] H. F. Levison, A. Morbidelli, K. Tsiganis, D. Nesvorný, and R. Gomes, “Late Orbital Instabilities in the Outer Planets Induced by Interaction with a Self-gravitating Planetesimal Disk,” *The Astronomical Journal*, Vol. 142, No. 5, 2011, p. 152.
- [2] M. Vavrina, J. Englander, and D. Ellison, “Global Optimization of N-Maneuver, High-Thrust Trajectories Using Direct Multiple Shooting,” *AAS/AIAA Space Flight Mechanics Meeting*, February 2016.
- [3] D. H. Ellison and J. A. Englander, “High-Fidelity Multiple-Flyby Trajectory Optimization Using Multiple Shooting,” *AAS/AIAA Astrodynamics Specialist Conference*, 2019.
- [4] D. H. Ellison, *Robust Preliminary Design for Multiple Gravity Assist Spacecraft Trajectories*. PhD thesis, May 2018.
- [5] “Systems Tool Kit,” <http://agi.com/products/engineering-tools>.
- [6] J. V. McAdams, K. E. Williams, J. A. Englander, D. H. Ellison, J. M. Knittel, D. B. Stanbridge, B. Sutter, and K. Berry, “Refining Lucy Mission Delta-V during Spacecraft Design using Trajectory Optimization within High-Fidelity Monte Carlo Maneuver Analysis,” *AAS/AIAA Astrodynamics Specialist Conference*, 2019.
- [7] “General Mission Analysis Toolkit,” <http://www.gmatcentral.org/>.

- [8] D. H. Ellison, B. A. Conway, J. A. Englander, and M. T. Ozimek, “Application and Analysis of Bounded-Impulse Trajectory Models with Analytic Gradients,” *Journal of Guidance, Control, and Dynamics*, Vol. 41, No. 8, 2018, pp. 1700–1714, 10.2514/1.G003078.
- [9] J. Prussing and B. Conway, *Orbital Mechanics*. Oxford University Press, New York, 1993.
- [10] G. J. Der, “Classical and Advanced Kepler Algorithms,” [http://deraastrodynamics.com/docs/kepler\\_algorithms\\_v2.pdf](http://deraastrodynamics.com/docs/kepler_algorithms_v2.pdf).
- [11] “SPICE Ephemeris,” <http://naif.jpl.nasa.gov/naif/>, accessed 6/26/2016.
- [12] P. E. Gill, W. Murray, and M. A. Saunders, “SNOPT: An SQP Algorithm for Large-Scale Constrained Optimization,” *SIAM J. Optim.*, Vol. 12, jan 2002, pp. 979–1006, 10.1137/s1052623499350013.
- [13] D. H. Ellison, B. A. Conway, J. A. Englander, and M. T. Ozimek, “Analytic Gradient Computation for Bounded-Impulse Trajectory Models Using Two-Sided Shooting,” *Journal of Guidance, Control, and Dynamics*, Vol. 41, No. 7, 2018, pp. 1449–1462, 10.2514/1.G003077.
- [14] C. H. Yam, D. D. Lorenzo, and D. Izzo, “Low-thrust trajectory design as a constrained global optimization problem,” Vol. 225, SAGE Publications, aug 2011, pp. 1243–1251, 10.1177/0954410011401686.
- [15] G. A. Rauwolf and V. L. Coverstone-Carroll, “Near-optimal low-thrust orbit transfers generated by a genetic algorithm,” *Journal of Spacecraft and Rockets*, Vol. 33, nov 1996, pp. 859–862, 10.2514/3.26850.
- [16] V. Coverstone-Carroll, “Near-Optimal Low-Thrust Trajectories via Micro-Genetic Algorithms,” *Journal of Guidance, Control, and Dynamics*, Vol. 20, jan 1997, pp. 196–198, 10.2514/2.4020.
- [17] V. Coverstone-Carroll, J. Hartmann, and W. Mason, “Optimal multi-objective low-thrust spacecraft trajectories,” *Computer Methods in Applied Mechanics and Engineering*, Vol. 186, jun 2000, pp. 387–402, 10.1016/s0045-7825(99)00393-x.
- [18] M. Vavrina and K. Howell, “Global Low-Thrust Trajectory Optimization Through Hybridization of a Genetic Algorithm and a Direct Method,” *AIAA/AAS Astrodynamics Specialist Conference and Exhibit*, AIAA, aug 2008, 10.2514/6.2008-6614.
- [19] J. A. Englander, B. A. Conway, and T. Williams, “Automated Mission Planning via Evolutionary Algorithms,” *Journal of Guidance, Control, and Dynamics*, Vol. 35, nov 2012, pp. 1878–1887, 10.2514/1.54101.
- [20] J. A. Englander, B. A. Conway, and T. Williams, “Automated Interplanetary Mission Planning,” *AAS/AIAA Astrodynamics Specialist Conference*, Minneapolis, MN, AIAA paper 2012-4517, August 2012, 10.2514/6.2012-4517.
- [21] J. A. Englander, *Automated Trajectory Planning for Multiple-Flyby Interplanetary Missions*. PhD thesis, University of Illinois at Urbana-Champaign, April 2013.
- [22] D. H. Ellison, J. A. Englander, and B. A. Conway, “Robust Global Optimization of Low-Thrust, Multiple-Flyby Trajectories,” *AAS/AIAA Astrodynamics Specialist Conference*, Hilton Head, SC, AAS paper 13-924, August 2013.
- [23] D. H. Ellison, J. A. Englander, M. T. Ozimek, and B. A. Conway, “Analytical Partial Derivative Calculation of the Sims-Flanagan Transcription Match Point Constraints,” *AAS/AIAA Space-Flight Mechanics Meeting*, Santa Fe, NM, AAS, January 2014.
- [24] J. A. Englander and A. C. Englander, “Tuning Monotonic Basin Hopping: Improving the Efficiency of Stochastic Search as Applied to Low-Thrust Trajectory Optimization,” *24th International Symposium on Space Flight Dynamics*, Laurel, MD, ISSFD, May 2014.
- [25] R. H. Leary, “Global Optimization on Funneling Landscapes,” *Journal of Global Optimization*, Vol. 18, No. 4, 2000, pp. 367–383, 10.1023/A:1026500301312.
- [26] B. Addis, A. Cassioli, M. Locatelli, and F. Schoen, “A global optimization method for the design of space trajectories,” *Computational Optimization and Applications*, Vol. 48, jun 2009, pp. 635–652, 10.1007/s10589-009-9261-6.
- [27] J. Englander, M. A. Vavrina, B. J. Naasz, R. G. Merrill, and M. Qu, “Mars, Phobos, and Deimos Sample Return Enabled by ARRM Alternative Trade Study Spacecraft,” *AIAA/AAS Astrodynamics Specialist Conference*, AIAA paper 2014-4354, aug 2014, 10.2514/6.2014-4354.
- [28] J. Knittel, K. Hughes, J. Englander, and B. Sarli, “Automated Sensitivity Analysis of Interplanetary Trajectories for Optimal Mission Design,” *International Symposium on Space Flight Dynamics*, Matsuyama, Japan, June 2017.